Temperature-dependent electronic structure and topological property of the Kondo semimetal CeFe$_2$Al$_{10}$

T.-S. Nam, Junwon Kim ●, Chang-Jong Kang ●,* Kyoo Kim,† and B. I. Min ●‡
Department of physics, Pohang University of Science and Technology, Pohang 37673, Korea

We have investigated the electronic structure and the topological property of a Ce Kondo system, CeFe$_2$Al$_{10}$, employing the first-principles density functional theory (DFT) and dynamical mean-field theory (DMFT) band calculations. Based on the DMFT band calculation, we have found that, upon cooling, Ce $4f$ electrons in CeFe$_2$Al$_{10}$ become coherent at $T \approx 150$ K, so as to form coherent bands revealing the hybridization pseudogap near the Fermi level (E_F). We have checked that the band structure near E_F and the Fermi surface from the DMFT at low T are almost identical with those from the renormalized DFT. We have explored the topological nature based on the DFT band structure and found that CeFe$_2$Al$_{10}$ has a topological Kondo insulating nature with $Z_4 = 1$. Therefore, our finding reveals that CeFe$_2$Al$_{10}$ would display T-dependent topological phase transition from a topological Kondo insulating phase at low T to a trivial semimetallic phase at high T. The analysis of T-dependent local magnetic susceptibility obtained from the DMFT calculation confirms the Kondo coherence mechanism upon cooling in CeFe$_2$Al$_{10}$.

I. INTRODUCTION

A recent report on the topological Kondo insulator has drawn a great deal of attentions [1–7], which then revived active followup researches on the Kondo insulators. The topological Kondo insulating phase is expected to emerge in heavy-fermion Kondo systems, in which a hybridization between coherent f electrons and usual conduction electrons induces the so-called "band inversion." This feature would appear below a specific temperature (T), namely, the coherent temperature T_{coh}, at which the localized f states start to form a coherent band via Kondo mechanism. SmB$_6$ was reported to be a promising candidate for a topological Kondo insulator, which exhibits the upturn and plateau in resistivity at low T. The upturn of resistivity is attributed to the Kondo effect, while the plateau behavior is thought to come from in-gap topological surface states (TSSs) [8,9].

CeM$_2$Al$_{10}$ (M=Fe, Ru, Os) exhibit anomalous behaviors in the resistivity, which are reminiscent of those in Kondo insulators. While CeRu$_2$Al$_{10}$ and CeOs$_2$Al$_{10}$ have antiferromagnetic orderings, CeFe$_2$Al$_{10}$ shows no magnetic ordering [10–12]. It is because CeFe$_2$Al$_{10}$ has a strong f-c (Ce $4f$ and conduction electrons) hybridization, which suppresses any possible magnetic ordering. Due to the strong hybridization, CeFe$_2$Al$_{10}$ is expected to have the largest real gap or pseudogap feature among CeM$_2$Al$_{10}$. Indeed, T-dependent resistivity shows a steep increase below $\sim$20 K, exhibiting a semiconducting behavior [11,13]. The pseudogap formation was identified by high-resolution photoemission spectroscopy (PES), manifesting the depletion of spectral weight near the Fermi level (E_F) with a gap size of 12 meV at 10 K [14]. The Kondo temperature (T_K) for CeFe$_2$Al$_{10}$ was estimated to be around $200 \sim 300$ K from the broad maximum of the magnetic susceptibility data [14,15]. CeFe$_2$Al$_{10}$ has also attracted recent attention due to a possible existence of spin exciton [15,16]. Inelastic neutron scattering measurement [16] showed the existence of a spin gap of 12.5 meV in the paramagnetic phase of CeFe$_2$Al$_{10}$. These experimental data are suggestive of a possible topological Kondo insulating nature for CeFe$_2$Al$_{10}$ like for SmB$_6$.

Most promising candidates for a topological Kondo insulator, such as SmB$_6$, Ce$_3$Pt$_3$Bi$_4$, YbB$_{12}$, have a cubic symmetry that does not provide any information on anisotropic hybridization. In contrast, Ce Kondo compounds having orthorhombic structure, such as CeNiSn [17,18] and CeFe$_2$Al$_{10}$, show highly anisotropic hybridizations between Ce $4f$ and conduction electrons. The evidences of the anisotropic hybridizations in CeFe$_2$Al$_{10}$ can be found in several experiments. Magnetic susceptibility along the a axis shows Curie-Weiss-like behavior at high T with broad maximum at 70 K and then decreases with decreasing T, whereas, along the b and c axes, T dependencies are weak in the entire T range, exhibiting $\chi_a > \chi_c > \chi_b$ [11–13,15]. Kondo semiconducting behavior of resistivity at low T is less pronounced along the c axis than those along the a and b axis [13]. An optical measurement showed different gap-formation temperatures for each axis, especially between ac plane and b axis [19]. Also the gap-opening temperature for each axis roughly coincides with the temperature where thermoelectric power has a maximum value [13]. These experiments indicate that the hybridization and Kondo effect in CeFe$_2$Al$_{10}$ are anisotropic.

*Present address: Department of Physics and Astronomy, Rutgers University, Piscataway, New Jersey, 08854, USA.

†Present address: Korea Atomic Energy Research Institute (KAERI), 111 Daedeok-daero, Daejeon 34057, Korea.
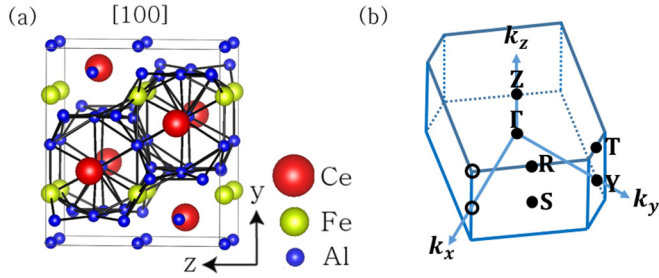
‡Corresponding author: bimin@postech.ac.kr

FIG. 1. (a) The orthorhombic crystal structure (*Cmcm* space group No. 63) of $CeFe_2Al_{10}$ viewed from the [100] direction. Bold black lines represent the Fe and Al cages surrounding Ce. (b) Brillouin zone (BZ) of the orthorhombic crystal structure.

In this study, we have investigated the electronic structure and the topological property of $CeFe_2Al_{10}$, employing the first-principles density functional theory (DFT) and dynamical mean-field theory (DMFT) band calculations [20,21]. Employing the DMFT band calculation, we have explored the T-dependent evolution of band structures to check how the Kondo effect is realized in $CeFe_2Al_{10}$. We have found that, upon cooling, Ce $4f$ electrons form a coherent band so as to reveal a hybridization gap (pseudogap) near E_F. We have determined the topological invariants based on the DFT band structure that is a good low-T manifestation of the DMFT band structure when f electrons form a coherent band. We have also studied the T-dependent behavior of local magnetic susceptibility based on the DMFT calculation.

II. COMPUTATIONAL DETAILS

$CeFe_2Al_{10}$ crystallizes in the orthorhombic structure of $YbFe_2Al_{10}$ type (*Cmcm* space group No. 63) [see Fig. 1(a)] [22]. There are total 26 atoms (2 Ce, 4 Fe, 20 Al atoms) in the unit cell. Ce atoms are located inside a cagelike polyhedral environment made of 4 Fe and 16 Al atoms. Fe atom has twelve neighbors of distorted icosahedral coordination (2 Ce and 10 Al) [23]. Ce and Fe ions are connected in a zigzag way on the *ac* plane [19]. We adopted the experimental lattice parameters of $a = 8.992$ Å, $b = 10.216$ Å, and $c = 9.065$ Å [24], and then internal atomic positions are fully relaxed.

We have performed the band calculations, employing the all-electron full-potential linearized augmented plane-wave (FLAPW) method, implemented in WIEN2K [25]. The generalized-gradient approximation (GGA) scheme is utilized for the DFT exchange-correlation functional [26], and the spin-orbit coupling (SOC) is included ("DFT + SOC"). We have also considered ten-times enhanced SOC ("DFT + SOC×10"), which shows a better agreement with the DFT + DMFT result near E_F than the DFT + SOC in the low T limit. The SOC enhancement is taken into account only for Ce f states. For the strongly-correlated electron systems, the DFT $+U$ method is often adopted. The DFT $+U$, however, fails to capture the coherent f-band feature near E_F, which gives incorrect band symmetries and an incorrect topological invariant. This is the reason why we employed the DFT + SOC×10 scheme [8,9]. We have also done an open-core calculation treating f electrons as core ("$4f$ open core") to simulate the electronic structure at high T limit, where f electrons become

completely incoherent and so do not participate in hopping. We used $11\times11\times8$ k-point mesh in the full BZ, and the product of R_{MT} and K_{max} was chosen as 8. To examine the irreducible representations of bands at the high-symmetry k points, we have also utilized the VASP2TRACE code [27] implemented in the Vienna *ab initio* simulation package (VASP) [28].

For the DMFT band structure calculations, we have used the charge self-consistent DFT + DMFT method implemented in the WIEN2K code [20]. Continuous-time quantum Monte Carlo (CTQMC) [29] was adopted for the DMFT impurity solver with onsite Coulomb $U = 6.0$ eV and Hund's coupling $J = 0.68$ eV with nominal double counting scheme for the Ce $4f$ electrons, which is found to describe the correlation effects of Ce $4f$ electrons well [30,31]. Local magnetic susceptibility is obtained by evaluating the spin-spin correlation function at the impurity site in the loop of CTQMC quantum-impurity solver [32].

III. RESULTS AND DISCUSSIONS

Figure 2 shows the band structures of $CeFe_2Al_{10}$, obtained in the DFT + SOC, DFT + SOC×10, and $4f$ open-core schemes. All three band structures show a semimetallic nature. In the DFT + SOC, there are Ce f states near E_F, which are split into $j = 5/2$ and $j = 7/2$ states by the SOC. It is seen that Fe $3d$ states near E_F are depleted due to the hybridization with Ce f states, manifesting a pseudogap feature. In the DFT + SOC×10, the large SOC shifts up the Ce $f_{7/2}$ states far above E_F, and so their overestimated contribution to the Fermi surfaces are expected to be minimized. As a consequence, the elongated electron Fermi surface along $\Gamma - Y$ in the DFT + SOC gets disconnected in the DFT + SOC×10, changing from the open Fermi surface to closed ones. We will see in Fig. 4 below that the Fermi surfaces obtained from the DFT + SOC × 10 are much closer to the DMFT Fermi surfaces than those obtained from the DFT + SOC. This feature suggests that the DFT + SOC × 10 simulates the DMFT band structure near E_F better than the DFT + SOC. On the other hand, in the $4f$ open-core scheme, due to the absence of f electrons, there are dispersive Fe d bands near E_F, which produce wide-spread Fermi surfaces, as shown in Fig. 2(i).

Figure 3 shows DMFT band structures and densities of states (DOSs) of $CeFe_2Al_{10}$ for different T's. At very high T (1500 K), Ce f electrons are incoherent, and so the states near E_F correspond to mostly Fe $3d$ states, as shown in Figs. 3(d) and 3(h). Upon cooling, Ce $4f$ states near E_F and spin-orbit split states at ∼0.4 eV develop with higher intensity, producing sharp Kondo resonance peaks in the DOS. At $T = 150$ K, Ce f electrons become sufficiently coherent so as to form the Ce $4f$ band near E_F and the spin-orbit-side band. With the $4f$ band formation, the hybridization gap opens near E_F through the f-c hybridization. But the gap is not large enough to make a system insulating. Namely, as shown in Fig. 5 below, there are a few bands cutting E_F in some part of BZ, and so only the V-shaped pseudogap is formed remaining as a semimetal.

In Fig. 4, the band structures near E_F and two-dimensional (2D) Fermi surfaces ($k_z = 0$) of $CeFe_2Al_{10}$ are compared between DFT and DMFT results. It is seen in Figs. 4(a)
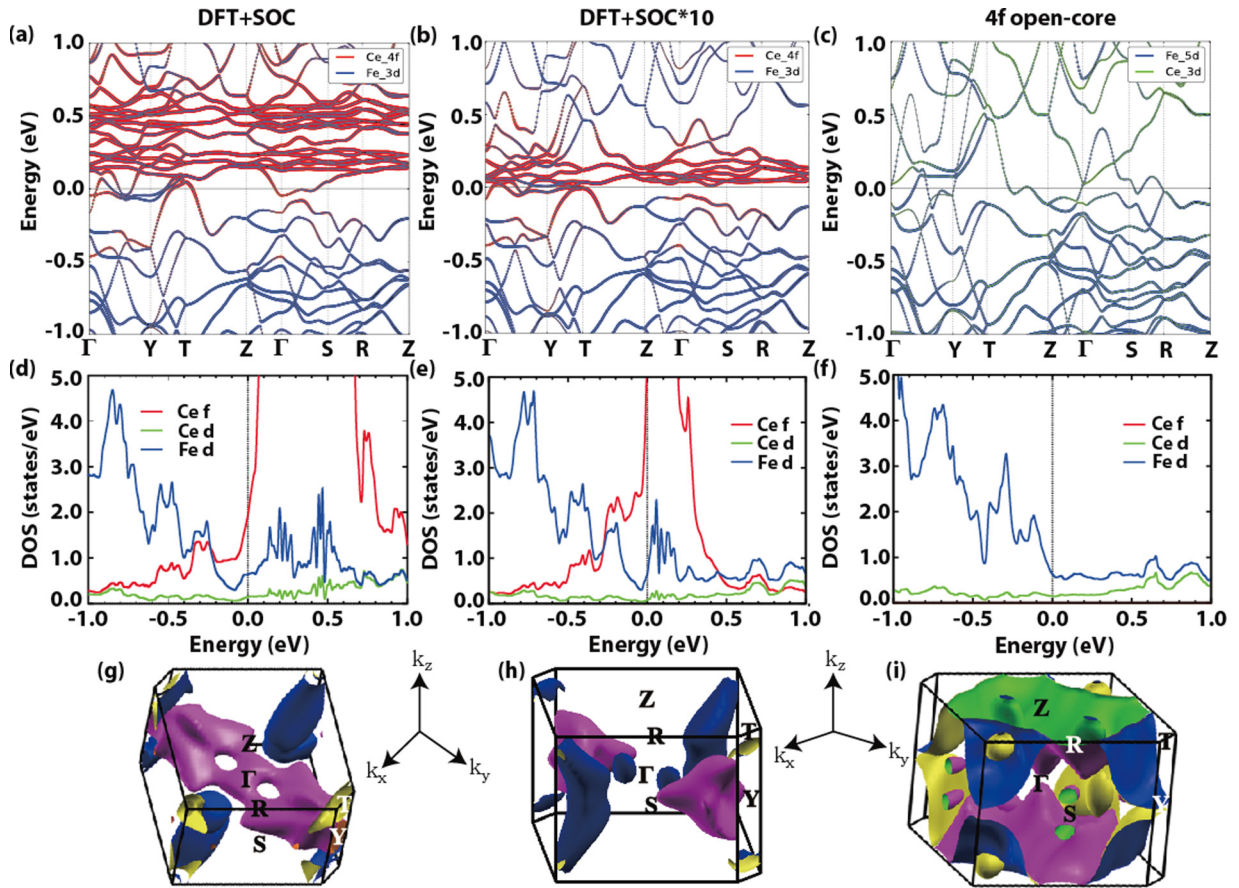
FIG. 2. Band structures (a)–(c), densities of states (d)–(f), and Fermi surfaces (g)–(i) of CeFe$_2$Al$_{10}$ obtained from DFT + SOC, DFT + SOC×10, and 4f open-core schemes, respectively. All the results show semimetallic nature, even though the Fermi surface volumes are reduced for the DFT + SOC and DFT + SOC×10 with respect to that for the 4f open core. The shapes of BZ's in (g)–(h) look different because of different viewpoints.

and 4(b) and Figs. 4(e) and 4(f) that band structure near E_F and Fermi surface from the DMFT at $T = 150$ K are almost identical with those from the DFT + SOC × 10 provided with

a proper bandwidth renormalization [33]. The renormalization factor $Z = 0.28$ is obtained from the DMFT self-energy at $T = 150$ K, which implies that the f bandwidth in the
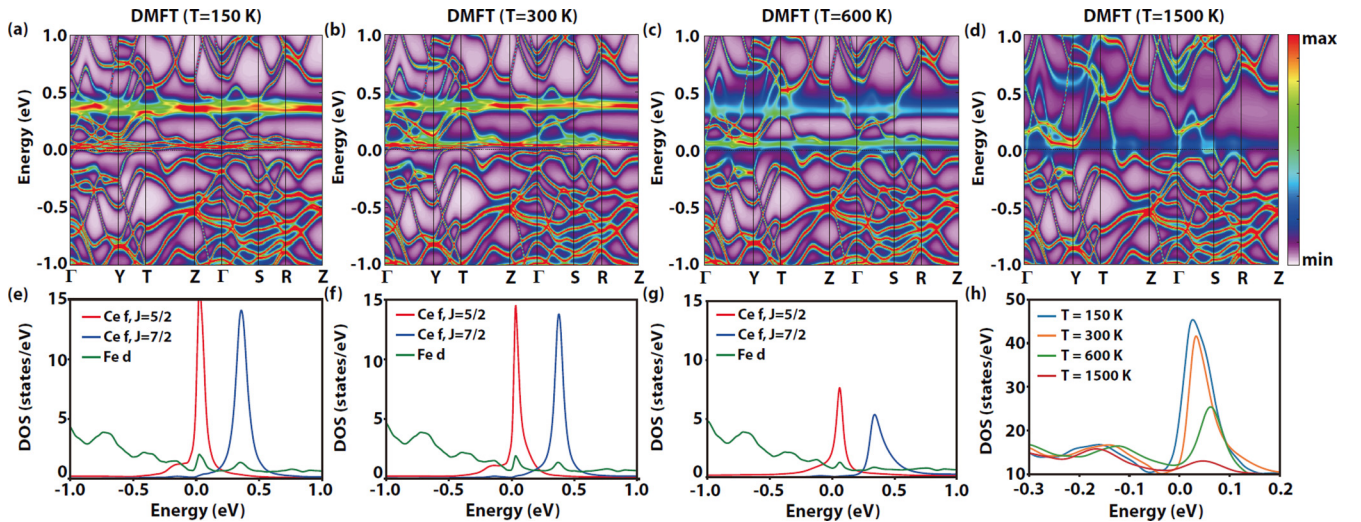

FIG. 3. (a)–(d) DMFT band structures and (e)–(h) DOSs of CeFe$_2$Al$_{10}$ at $T = 150$ K, 300 K, 600 K, and 1500 K. For the DOSs, Ce $f_{5/2}$ and $f_{7/2}$ components and Fe d component are provided, and in (h), total DOSs for different T's are compared. Upon cooling, Ce f bands in (a)–(d) are seen to become coherent and hybridized with dispersive Fe d band, producing the hybridization gap near E_F, as shown in (h).
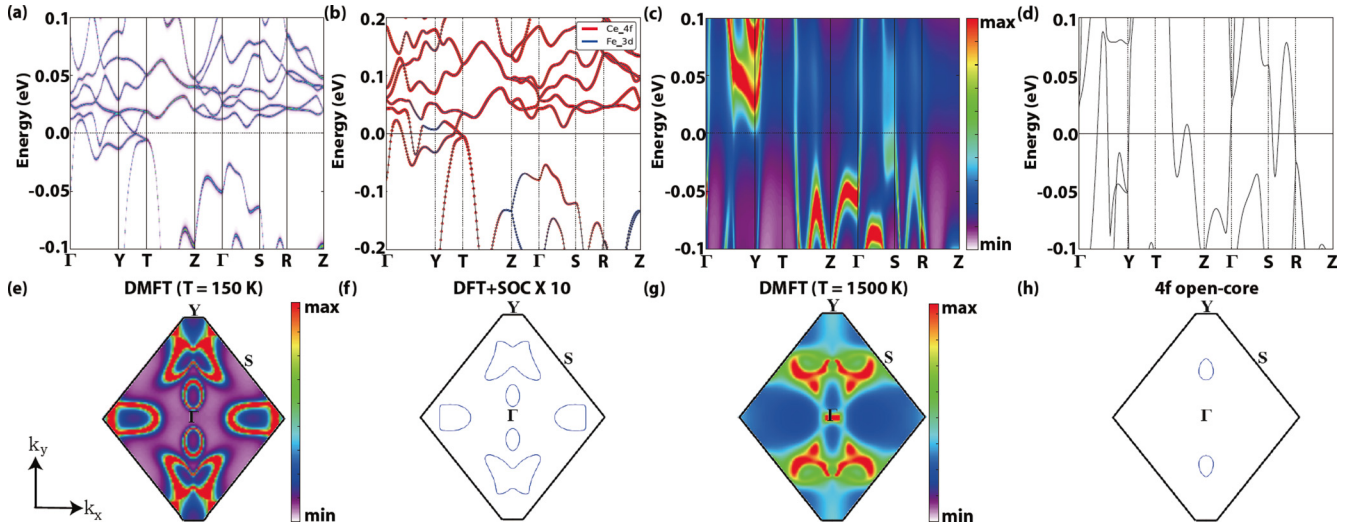
FIG. 4. Comparison of band structures of $CeFe_2Al_{10}$ between DMFT and DFT schemes: (a) DMFT at $T = 150$ K, (b) DFT $+ SOC \times 10$, (c) DMFT at $T = 1500$ K, and (d) $4f$ open-core. (e)–(h) Comparison of 2D Fermi surfaces ($k_z = 0$) between DMFT and DFT schemes: (e) DMFT at $T = 150$ K, (f) DFT $+ SOC \times 10$, (g) DMFT at $T = 1500$ K, and (h) $4f$ open-core. In (a), the imaginary part of self-energy is set to be zero to show the band dispersion more clearly. At low T, both the band structures near E_F (a) and (b) and Fermi surfaces (e) and (f) are almost identical between DMFT ($T = 150$ K) and DFT $+ SOC \times 10$, indicating that the renormalized DFT bands would describe well the low T band structure of $CeFe_2Al_{10}$. The DMFT band structure at high T (1500 K) in (c) matches will with the $4f$ open-core band structure in (d), reflecting that Ce f electrons become incoherent at high T. Corresponding Fermi surfaces show features similar to each other, but also show nonnegligible f-c hybridization even at such high T.

DMFT is narrower than that in the DFT by $Z = 0.28$ factor. This agreement indicates that (i) Ce $4f$ electrons in $CeFe_2Al_{10}$ become almost coherent at $T = 150$ K, and (ii) the DFT, especially the DFT $+ SOC \times 10$, describes properly the near E_F band structure of $CeFe_2Al_{10}$ at low T. On the other hand, Figs. 4(c) and 4(d) show that the DMFT band structure at high T (1500 K) is very close to the band structure obtained from the $4f$ open-core calculation, suggesting that Ce $4f$ are incoherent so as to be localized at high T. Dispersive Fe $3d$ bands in the $4f$ open-core calculation are reflected well in the DMFT band structure at high T. As shown in Figs. 4(g) and 4(h), Fermi surfaces of the DMFT at high T and $4f$ open-core calculations show features similar to each other, but also show non-negligible f-c hybridization in DMFT Fermi surfaces even at such high T.
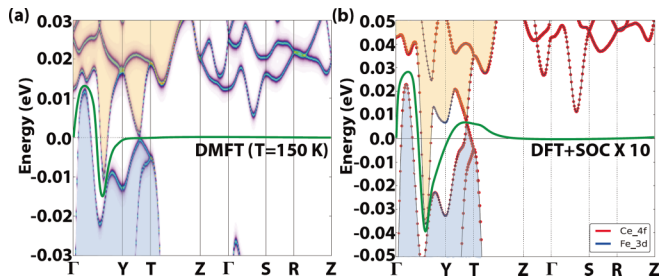

FIG. 5. The amplified band structures of $CeFe_2Al_{10}$: (a) DMFT at $T = 150$ K and (b) DFT $+ SOC \times 10$. For both cases, full-gap openings are shown to exist between bands above and below the fictitious chemical potential denoted by green lines, and thereby the topological invariant can be obtained from the bands below that chemical potential.

Even though both DFT and DMFT band structures of $CeFe_2Al_{10}$ have semimetallic nature at low T, we can investigate its topological character by setting a fictitious chemical potential in between two bands separated out through all k points and then obtaining the topological invariant from the bands below that chemical potential. We have checked that the topological Hamiltonian introduced in Ref. [34] produces the almost identical band structure to that of DFT $+ SOC \times 10$, suggesting that topological invariants can be determined from the DFT $+ SOC \times 10$ band structure. As shown in Fig. 5, both band structures from the DMFT at $T = 150$ K and the DFT $+ SOC \times 10$ have the full gap between the two bands producing the electron and hole pockets, respectively. The existence of band gap along Y-T, albeit tiny, is assured by the band symmetry, because all the bands along Y-T have the same irreducible representation of H_5. Then, as in conventional topological insulators, we can determine the topological invariant of $CeFe_2Al_{10}$, applying the VASP2TRACE code to the DFT $+ SOC \times 10$ band structure. We employed the DFT $+ SOC \times 10$ band structure rather than the DFT $+ SOC$ band structure because the former simulates more properly the DMFT band structure near E_F.

For the $Cmcm$ space group (No. 63) of $CeFe_2Al_{10}$, which has the time-reversal symmetry and the strong SOC, there are four topological indices of Z_{2w} and Z_4 [27,35,36]. Since $CeFe_2Al_{10}$ has the inversion symmetry, these topological indices can be determined by analyzing parities of the occupied bands below the fictitious chemical potential at the time-reversal invariant momentum (TRIM) k points [36,37]. The resulting topological indices we have obtained based on the DFT $+ SOC \times 10$ band structure are $(Z_{2w,1}, Z_{2w,2}, Z_{2w,3}) = (1, 1, 0)$ and $Z_4 = 1$. Here Z_{2w}'s correspond to the weak topological-insulator (TI) indices, while $Z_4 = 1$ corresponds
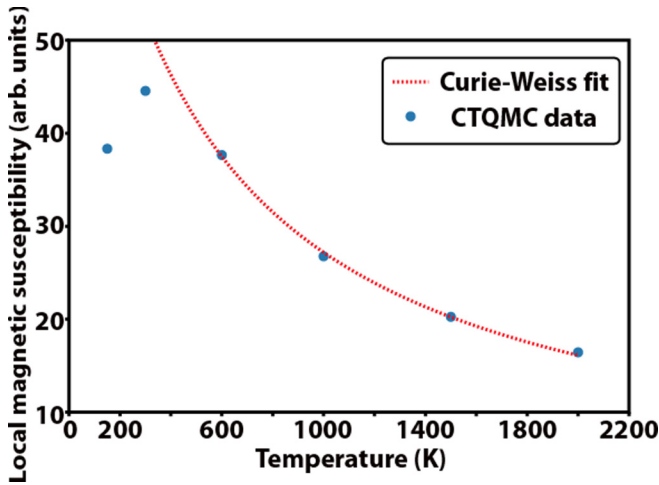
FIG. 6. T-dependent local magnetic susceptibility (arbitrary unit) obtained from the DMFT calculation. Susceptibility data at high T fit well into the antiferromagnetic Curie-Weiss curve, $\chi_m = C/(T + \theta)$ with $\theta \approx 455$ K, but start to deviate from the curve below 300 K.

to the strong TI index in the presence of inversion symmetry [36,38], indicating that CeFe$_2$Al$_{10}$ would be a strong TI in the ground state. By contrast, for the $4f$ open-core case, we cannot determine the topological invariant because of an absence of fully-gapped band structure near E_F. As discussed in Fig. 4, the topological nature obtained from the DFT band structure is expected to be consistent with that from the DMFT band structure, suggesting that topological character would be changed by varying T. Namely, CeFe$_2$Al$_{10}$ would exhibit T-dependent topological phase transition from a topological $Z_4 = 1$ Kondo insulating phase at low T to a trivial semimetallic phase at high T.

Figure 6 provides T-dependent local magnetic susceptibility, obtained in the CTQMC loop of DMFT calculation [32]. The susceptibility shows the increasing behavior upon cooling, manifesting a peak at $T = 300$ K, and then appears to decrease below $T = 300$ K. As shown in Fig. 6, the calculated susceptibility data at high T are fitted well into an antiferromagnetic Curie-Weiss formula of $\chi_m = C/(T + \theta)$ with $\theta \approx 455$ K, indicating that Ce f electrons behave as localized spins above $T = \theta$. The susceptibility starts to deviate

from the Curie-Weiss curve below $T = 300$ K. This feature suggests that localized spins start to be compensated by the conduction electrons below $T = 300$ K. Indeed, this behavior is quite consistent with that in the observed magnetic susceptibility [22], even though the peak position in the latter is rather low, around $T = 80$ K. This difference is expected to come from the applied magnetic field, $B = 0.3$ T, in the experiment, which is not considered in the calculation. The T-dependent behavior of local magnetic susceptibility in Fig. 6 provides clear evidence for the Kondo crossover upon cooling from local to coherent states of Ce f electrons.

IV. CONCLUSIONS

We have investigated T-dependent electronic structures and topological properties of the Kondo compound, CeFe$_2$Al$_{10}$. CeFe$_2$Al$_{10}$ is obtained to be a semimetal in the ground state. The DMFT calculation shows that Ce $4f$ electrons become coherent, upon cooling, so as to form f band that makes the hybridization with dispersive Fe d bands. The hybridization-induced pseudogap appears in the DOS near E_F with V-shaped dip feature. CeFe$_2$Al$_{10}$ has a topological Kondo insulating nature with a topological invariant of $Z_4 = 1$. Hence CeFe$_2$Al$_{10}$ would have a T-dependent topological phase transition from a trivial semimetal at high T to a topological Kondo insulator at low T. The T-dependent behavior of local magnetic susceptibility is consistent with the coherent band formation of Ce f electrons upon cooling in CeFe$_2$Al$_{10}$. The TSSs in CeFe$_2$Al$_{10}$ are expected to submerge into the bulk-projected bands, and so the identification of TSSs would be challenging in ARPES measurement. But it is expected that TSSs would induce interesting transport properties, such as ultrahigh mobility due to protected surface states and the Berry-phase-induced anomalous magnetoresistance, which can be utilized for the possible application to the spintronic devices.

[1] M. Dzero, K. Sun, V. Galitski, and P. Coleman, Phys. Rev. Lett. **104**, 106408 (2010).

[2] F. Lu, J. Z. Zhao, H. Weng, Z. Fang, and X. Dai, Phys. Rev. Lett. **110**, 096401 (2013).

[3] X.-Y. Feng, J. Dai, C.-H. Chung, and Q. Si, Phys. Rev. Lett. **111**, 016402 (2013).

[4] X. Deng, K. Haule, and G. Kotliar, Phys. Rev. Lett. **111**, 176404 (2013).

[5] H. Weng, J. Zhao, Z. Wang, Z. Fang, and X. Dai, Phys. Rev. Lett. **112**, 016403 (2014).

[6] P.-Y. Chang, O. Erten, and P. Coleman, Nat. Phys. **13**, 794 (2017).

[7] C. Cao, G.-X. Zhi, and J.-X. Zhu, Phys. Rev. Lett. **124**, 166403 (2020).

[8] J. Kim, K. Kim, C.-J. Kang, S. Kim, H. C. Choi, J.-S. Kang, J. D. Denlinger, and B. I. Min, Phys. Rev. B **90**, 075131 (2014).

[9] C.-J. Kang, J. Kim, K. Kim, J. Kang, J. D. Denlinger, and B. I. Min, J. Phys. Soc. Jpn. **84**, 024722 (2015).

[10] T. Nishioka, Y. Kawamura, T. Takesaka, R. Kobayashi, H. Kato, M. Matsumura, K. Kodama, K. Matsubayashi, and Y. Uwatoko, J. Phys. Soc. Jpn. **78**, 123705 (2009).

[11] Y. Muro, K. Yutani, J. Kajino, T. Onimaru, and T. Takabatake, J. Korean Phys. Soc. **63**, 508 (2013).

[12] F. Strigari, T. Willers, Y. Muro, K. Yutani, T. Takabatake, Z. Hu, S. Agrestini, C.-Y. Kuo, Y.-Y. Chin, H.-J. Lin, T. W. Pi, C. T. Chen, E. Weschke, E. Schierle, A. Tanaka, M. W. Haverkort, L. H. Tjeng, and A. Severing, Phys. Rev. B **87**, 125119 (2013).

[13] H. Tanida, M. Nakamura, M. Sera, A. Kondo, K. Kindo, T. Nishioka, and M. Matsumura, J. Phys. Soc. Jpn. **83**, 084708 (2014).

[14] T. Ishiga, T. Wakita, R. Yoshida, H. Okazaki, K. Tsubota, M. Sunagawa, K. Uenaka, K. Okada, H. Kumigashira, M. Oshima, K. Yutani, Y. Muro, T. Takabatake, Y. Muraoka, and T. Yokoya, J. Phys. Soc. Jpn. **83**, 094717 (2014).

[15] D. T. Adroja, A. D. Hillier, Y. Muro, T. Takabatake, A. M. Strydom, A. Bhattacharyya, A. Daoud-Aladin, and J. W. Taylor, Phys. Scr. **88**, 068505 (2013).

[16] D. T. Adroja, A. D. Hillier, Y. Muro, J. Kajino, T. Takabatake, P. Peratheepan, A. M. Strydom, P. P. Deen, F. Demmel, J. R. Stewart, J. W. Taylor, R. I. Smith, S. Ramos, and M. A. Adams, Phys. Rev. B **87**, 224415 (2013).

[17] T.-S. Nam, C.-J. Kang, D.-C. Ryu, J. Kim, H. Kim, K. Kim, and B. I. Min, Phys. Rev. B **99**, 125115 (2019).

[18] C. Bareille, T.-S. Nam, T. Takabatake, K. Kuroda, T. Yajima, M. Nakayama, S. Kunisada, S. Akebi, M. Sakano, S. Sakuragi, R. Noguchi, B. I. Min, S. Shin, and T. Kondo, Phys. Rev. B **100**, 045133 (2019).

[19] S. Kimura, Y. Muro, and T. Takabatake, J. Phys. Soc. Jpn. **80**, 033702 (2011).

[20] K. Haule, C.-H. Yee, and K. Kim, Phys. Rev. B **81**, 195107 (2010).

[21] G. Kotliar, S. Y. Savrasov, K. Haule, V. S. Oudovenko, O. Parcollet, and C. A. Marianetti, Rev. Mod. Phys. **78**, 865 (2006).

[22] Y. Muro, K. Motoya, Y. Saiga, and T. Takabatake, J. Phys. Soc. Jpn. **78**, 083707 (2009).

[23] S. Niemann and W. Jeitschko, Z. Kristallogr. **210**, 338 (1995).

[24] V. M. Thiede, T. Ebel, and W. Jeitsschko, J. Mater. Chem. **8**, 125 (1998).

[25] P. Blaha, K. Schwarz, G. K. H. Madsen, D. Kavasnicka, and J. Luitz, *Wien2k* (Karlheinz Schwarz, Technische Universitat Wien, Austria, 2001).

[26] J. P. Perdew, K. Burke, and M. Ernzerhof, Phys. Rev. Lett. **77**, 3865 (1996).

[27] M. G. Vergniory, L. Elcoro, C. Felser, N. Regnault, B. A. Bernevig, and Z. Wang, Nature (London) **566**, 480 (2019).

[28] G. Kresse and J. Furthmüller, Comput. Mater. Sci. **6**, 15 (1996).

[29] K. Haule, Phys. Rev. B **75**, 155113 (2007).

[30] J.-W. Kim, D.-C. Ryu, C.-J. Kang, K. Kim, H.-C. Choi, T.-S. Nam, and B. I. Min, Phys. Rev. B **100**, 195138 (2019).

[31] D.-C. Ryu, J.-W. Kim, K. Kim, C.-J. Kang, J. D. Denlinger, and B. I. Min, Phys. Rev. Res. **2**, 012069(R) (2020).

[32] Local magnetic susceptibility χ_m is obtained by using $\chi_m = \int_0^\beta \langle m_z(\tau) m_z(0) \rangle d\tau$, where m_z is the local magnetic moment of cerium atom and β is the inverse T. See K. Haule and G. Kotliar, New J. Phys. **11**, 025021 (2009).

[33] The DFT + SOC yields the open-orbit Fermi surface elongated along $\Gamma - Y$, which is quite different from the closed-orbit Fermi surfaces obtained from the DMFT.

[34] Z. Wang and B. Yan, J. Phys.: Condens. Matter **25**, 155601 (2013).

[35] H. C. Po, A. Vishwanath, and H. Watanabe, Nat. Commun. **8**, 50 (2017).

[36] Z. Song, T. Zhang, Z. Fang, and C. Fang, Nat. Commun. **9**, 3530 (2018).

[37] L. Fu and C. L. Kane, Phys. Rev. B **76**, 045302 (2007).

[38] E. Khalaf, H. C. Po, A. Vishwanath, and H. Watanabe, Phys. Rev. X **8**, 031070 (2018).